# NASA Technical Memorandum 102691

# VIDEO PHOTOGRAPHIC CONSIDERATIONS FOR MEASURING THE PROXIMITY OF A PROBE AIRCRAFT WITH A SMOKE SEEDED TRAILING VORTEX

BROOKS A. CHILDERS AND WALTER L. SNOW

JUNE 1990



National Aeronautics and Space Administration

**Langley Research Center**
Hampton, Virginia 23665-5225

## Introduction

One impediment to increasing landing capacity at large airports is the longitudinal separation required between aircraft to avoid wake vortex encounters which could cause flow-induced upsets of trailing aircraft. An effective warning system to detect the proximity of a vortex would allow relaxing the conservative standard now used to insure vortex dissipation and thus increase airport traffic throughput. A feasibility study by Continuum Dynamics Inc. (CDI) [See reference 1.] proposes an on-board wake vortex avoidance system which uses state-of-the-art sensors (e.g. flow direction vanes, roll rate gyros, accelerometers) to detect the proximity of a vortex. To be effective the scheme must detect vortices far enough away to allow time for the pilot to complete avoidance maneuvers. NASA's Langley Research Center (LaRC) agreed to collaborate with FAA's Langley Engineering Field Office and the NASA Wallops Flight Facility (WFF) in a simple flight investigation to assess the advisability of continued funding of the CDI effort (Reference 2).

A crucial aspect of the proposed investigation is to use an independent scheme to continuously monitor the encounter separation to correlate with the probe aircraft's sensor data. The analytical model in reference 1 treats the trailing vortex system to dipole approximation and predicts the maximum distance at which the vortex can be detected as a function of generating aircraft weight. This paper discusses the video based optical technique used to measure probe aircraft-vortex core separation. The technique circumvents most of the distortion and scaling error which would be involved in making such measurements directly from a television monitor faceplate.

### Symbols

| | |
|---|---|
| $c$ | focal length of camera lens, mm |
| $d$ | image of $D$ on photograph, mm |
| $D$ | distance between the center of gravity of the probe aircraft and the vortex core, ft |
| $h$ | nominal altitude of probe aircraft and trailing vortex, ft |
| $R$ | range to probe aircraft from camera on photo aircraft, ft |
| $w$ | image of $W$, mm |
| $W$ | wingspan of probe aircraft, ft |
| $\Delta h$ | nominal vertical separation distance between photo aircraft and probe aircraft, ft |
| $\theta$ | acute angle between vortex core and flight path of probe aircraft, radians |

## Measurement Concept

In an earlier LaRC study (Reference 3) a photogrammetric approach using entrained balloons for measuring the location of a vortex core in space was proposed. The method keys on the low-pressure nature of the vortex core which is known to attract neutral buoyancy tracers in aerodynamic studies. Balloons launched from an aircraft would be entrained in the cores of its wing tip trailing vortices. Standard photogrammetric triangulation techniques would then be used to locate the balloons demarcating the cores. Reference 3 cites prior evidence of balloon entrainment in aircraft wakes and describes laboratory mock-ups to assess the accuracy of the method.

A single experiment was performed at WFF using a Short Aircraft Company Skyvan aircraft to attempt balloon entrainment. The aircraft has a large hatch door in the aft of the fuselage from which balloons were released in flight. Only a few of several hundred balloons released were captured by the core. It was realized that the probability of core capture would be greatly enhanced if deployment were possible in the vicinity of the wing tips. Deferring to expediency it was decided to fall back to a single camera, constrained photogrammetry, solution using smoke instead of balloons for core demarcation. The constraint in this case assumes that the encounter aircraft and vortex are at the same altitude. This affords a single camera solution since the separation of the probe aircraft from the core can be found by image plane measurements once the scale of the photograph is determined. Wing tip smokers installed on the aircraft generating the vortex were used to delineate the cores. A camera equipped observation aircraft was used to photograph the encounter of the instrumented probe aircraft with the smoke defined vortex core(s). Figure 1 is a diagram of the experiment. The generator aircraft is equipped with wing tip smokers. The single engined probe aircraft flies approximately level with the trailing vortex at an altitude h which is about 5000 feet so that the pilot can recover from a vortex-induced upset. The photo aircraft flies above the probe aircraft ($\Delta h \approx 500 feet$) and is equipped with wing tip cameras to survey the scene. The top part of the figure shows the probe aircraft encountering the core at a shallow angle $\theta$. The purpose of the photo mission is to record $D(t)$ to correlate with sensor measurements on the probe aircraft. Figure 2 is a picture of the Lockheed P-3 which served to generate the vortex and Figure 3 shows the aircraft in flight with both wing tip smoke generators turned on. Figure 4 is a picture of the Piper PA-28 probe airplane and Figure 5 is the Beech T-34 which served as the photo aircraft. In the absence of aberrations, the situation is described mathematically as a perspective transformation, i.e. all rays from an object proceed through a perspective center and intercept the photosensitive surface. Figure 6

shows the idealized geometry. Notice that the direction of a ray is not changed in traversing the perspective center. Within the framework of first order Gaussian optics two nodal points are defined such that an oblique ray directed toward the first nodal point appears to emerge from the second parallel to its original direction. In practice the perspective center is identified with the rear nodal point of a camera lens. Electro-optical distortions introduced by the imaging lens and sensor architecture are determined through a separate laboratory calibration and can be corrected. The required separation distance $D(t)$ can be determined from measurements on the image $d$ once the scale of the photograph is known.

## Equipment Considerations

In this study, miniature color solid state cameras were used. The active sensor is comprised of a matrix of 570 horizontal by 485 vertical active elements arrayed over a 6.39 by 4.88 mm. format. The camera acquired data at standard video framing rates (30 Hz) and was electronically shuttered to provide 1/1000 second exposures. The camera head is cylindrical in shape with a diameter of 17.5 mm and a length of 52.9 mm and is small enough to be contained within the wing tip of the T-34 photo airplane. Figure 7 shows the right wing camera location and mounting arrangement. The wing tips were modified with peepholes for the cameras without additional optical material that might have added distortion characteristics not accounted for in the laboratory calibration. Wing tip cameras were toed in slightly to provide overlapping coverage at 500 feet. This was accomplished in the hanger by establishing a line on the floor determined by plumb lines originating at the wing tip camera locations. The camera frames were centered on the reference line with the toe-in angle adjusted to give overlapping fields at the nominal 500 feet working distance.

Cameras were mounted on each wing tip to experiment with triangulation techniques in anticipation of experiments described in reference 2. For this report only single camera observations were needed so that the second camera served primarily to provide a redundant data set. A time code (accurate to milliseconds) was inserted into the video signal and each wing tip camera was recorded on its own super VHS recorder. Figure 8 shows a schematic diagram of the photo acquisition system. This figure also indicates a fuselage camera. Skilled piloting was required to accomplish the formation flying for this mission. To account for the fact that the action was taking place directly beneath the photo airplane and therefore not visible by the pilot, a co-pilot viewed a third downlooking camera on

a cockpit monitor. The fuselage camera had a slightly larger field of view than either wing tip camera. The co-pilot was thus able to relay course correction information to keep the cameras roughly centered on the scene. A typical frame of data is shown in figure 9. It was photographed from a video monitor and shows the instrumented probe aircraft within a wing span or so of the vortex core. The time code is visible on the picture and was used to correlate with other sensor data.

## Data Reduction

The idealized measurement depicted in figure 6 is compromised by several practical considerations. In the first place the mapping is nonlinear due to the presence of the camera lens. In particular, the short focal length lens (8mm) required to get broad field coverage resulted in severe radial distortion. Figure 10 maps the distortion characteristics of the left wing tip camera. The camera was calibrated by viewing a known object field from different perspectives under laboratory conditions. Parameters to account for radial and decentering distortion were varied to make the data sets consistent in a least squares sense. This approach is known in the photogrammetry literature [See reference 4.] as analytic self calibration. Once the parameters are determined, any raw image coordinate can be corrected geometrically using an algebraic equation involving the measured parameters. Figure 10 represents the active sensor area of one solid state camera. The aspect ratio is consistent with the 4:3 format of standard television monitors. The open diamond represents the geometric center of the sensor while the square represents the optical axis reference point determined through self calibration. Optical distortion typically displays symmetry about the optical axis. The solid circles represent the positions of a set of points arrayed along the border of a square in object space given the idealized geometry of figure 6. The open circles show how the points are actually mapped due to the lens. The (predominantly barrel) distortion is clearly evident. Contours of equal distortion are also shown on the plot. The contour interval was chosen to correspond to a 10 foot displacement error at the nominal working distance of 500 feet for this experiment. Notice that the correction is an algebraic quantity. Distances measured between adjacent points in the image could be reasonably accurate even though both end points have large bias errors. For points located in opposite extremes of the image, however, bias error would not cancel. In this report all image data has been corrected for geometric distortion.

A remaining source of error is not so easily quantified and involves establishing the photographic scale of the

image. To determine the distance to the vortex center D (See figure 6.) by measuring its distance $d$ on the image, the scale of the photo must be known. If the range R were known (e.g. by triangulation ), then the scale would be c/R where c is the camera constant (nominally the focal length) which is also found by calibration. Alternatively, the scale may be found by measuring the image dimension of a known length in the field. The wingspan W and its image w were used for this purpose. For $\frac{w}{W}$ to equal $\frac{c}{R}$ the geometric plane containing the planform of the aircraft wing must be parallel to the image plane. This is assumed for the data readout and it is incumbent on the pilot of the probe aircraft to maintain altitude with the smoke trail (See figure 1.) to justify the assumption. The bias error associated with an altitude difference between the vortex and probe airplane can be evaluated for a specific measurement geometry. Bilanin's dipole [Ref. 1.] model restricts meaningful core distances to values exceeding 100 feet (the wingspan of the P-3 generating aircraft). For D=100 feet, R=500 feet, and an altitude difference of 20 feet, the bias error, disregarding roll, could contribute a 6% core distance measurement error.

The solid state camera's photosensitive surface is a two-dimensional array of semitransparent gates. Photons impinging on the sensor generate electrons in proportion to the light intensity. Packets of electrons associated with each picture element [pixel] are gated out of the device to create a video signal from which the image can be reconstructed. Conventional image acquisition boards map the signal strength to 8 bits so that a pixel receiving no light maps to 0 and a pixel saturated with light maps to 255. Figure 11 is a contour plot of a subset of pixels from figure 9. The plot roughly corresponds to the dashed area in figure 9. A listing of pixel intensities within the dashed rectangle in figure 11a is shown as figure 11b to illustrate how the image is stored digitally. The lowest contour plotted in figure 11a was chosen well above the background to avoid clutter. This accounts for the apparent separation of the tail from the airplane. The aircraft had a black band aft of the cockpit (See figure 4.) which reflected little light and would only be visible if a lower threshold were used for contouring. The unavoidable stair-stepping evident in the wing image occurs whenever edges are not aligned with the rows and columns of sensor elements. The density of sensor elements is chosen by the manufacturer to render acceptable visual images on a television monitor. The human visual process involves complicated image processing functions and incorporates some degree of smoothing. Figure 12 represents the figure 11 data with some nearest neighbor smoothing to roughly mimick the visual appearance of the image. The point to be made is that although the wingspan W is unambiguously determined during fabrication, the corresponding measurement $w$ on the image is not so straightforward and requires some judgement. Measurement of identical frames by independent observers suggest that repeatability errors correspond to about 1 pixel in calculating

$w$. This amounts to 2 or 3 percent scale error for the working range of these experiments. Repeatability or consistency is not accuracy, however, and independent tests would be required to uncover any biases.

In figure 13 the data set is shifted to incorporate both wing and vortex. For the atmospheric conditions encountered in data flights, the vortex core was reasonably well defined. Nevertheless, the distance to the "ridge" also requires estimation. Having made the scale determination, one still is faced with a judgment about how far the contour intervals representing the probe aircraft are from the contours representing the vortex.

Data was available at framing rates (30 Hz) for post-flight analysis. Photoanalysis involved playback on a video tape recorder interfaced with a personal computer. The PC-based image acquisition system is the one used in the LaRC Digital Video Model Deformation System and is described in reference 5. Having decided on a time interval for which both imagery and sensor data were acceptable, the operator could freeze frame selected images and perform the scaling and core distance estimation on the data. Figure 14 represents a summary of photodata for a particular encounter sequence from both wing tip cameras. Since both cameras recorded the same scene, the spread in measurements is an indicator of the judgmental uncertainties mentioned earlier. It is probably safe to assume that the measurements reported herein are reliable to 5% if the probe airplane and vortex are at a common altitude and possibly twice that much for altitude discrepancies of 20 feet.

## Concluding Remarks

Miniature solid state cameras were calibrated in the laboratory using analytical photogrammetric techniques to characterize distortion. The cameras were installed in the wing tips of a Beech T-34 photo airplane to view the interaction of an instrumented probe aircraft with a smoke seeded trailing vortex. Time code information was injected into the video signal to correlate with on-board sensors. PC-driven frame grabber technology and customized software were used to select and process particular tape recorded video fields after the flight. The image data was scaled by using the known wingspan of the probe aircraft.

The technique circumvents most of the distortion and scaling error which would be involved in making such measurements directly from a television monitor faceplate. The inaccuracy of the measurement is estimated to be on the order of 5% if the probe aircraft and vortex are at the same altitude and could be as much as 10% for altitude discrepancies of 20 feet. The analytical techniques reported in this paper constitute an integral part of the data

analysis of reference 2.

## References

1. Bilanin, Alan J.; Teske, Milton E.; and Curtiss, Howard C., Jr.: Feasibility of an Onboard Wake Vortex Avoidance System. C.D.I. Report No. 87-02 Continuum Dynamics, Inc. P.O. Box 3073, Princeton, New Jersey 08543. April, 1987.

2. Hastings, Earl C.; Patterson, James C.; and Verstynen, Harry A.: Airborne Vortex Detection Flight Test to Determine the Lateral Detection Distance. NASA TM 102672 FAA Report FAA-PM-RD-90. June, 1990.

3. Snow, Walter L.; Burner, Alpheus W.; and Goad, William K.: Photogrammetric Technique Using Entrained Balloons for In-Flight Ranging of Trailing Vortices. NASA TM 4129, October 1989.

4. Brown, Duane C.: Application of Close-Range Photogrammetry to Measurements of Structures in Orbit, Volume 2, GSI Tech. Rep. No. 80-012 (Contract No. MOM7DNS-895942), Geodetic Services Inc., Sept. 15, 1980.

5. Burner, A. W.; Snow, W.L.; Goad, W.K.; and Childers, B.A.: A Digital Video Model Deformation System. ICIASF '87, IEEE Catalog No. 87CH2449-7, Inst. of Electrical and Electronics Engineers, Inc., c.1987, pp. 210-220.

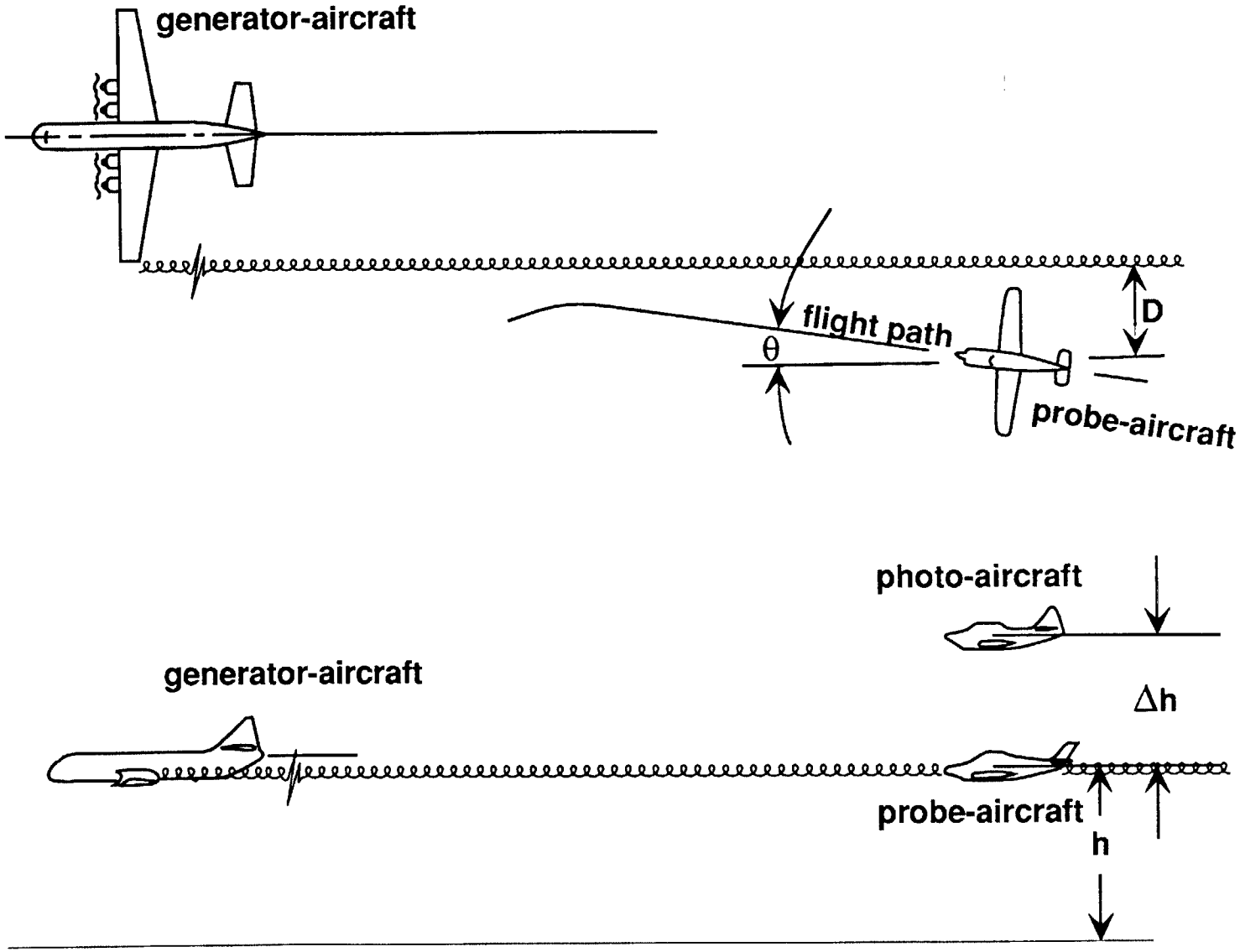


Figure 1. Top and side sketches of the measurement concept.

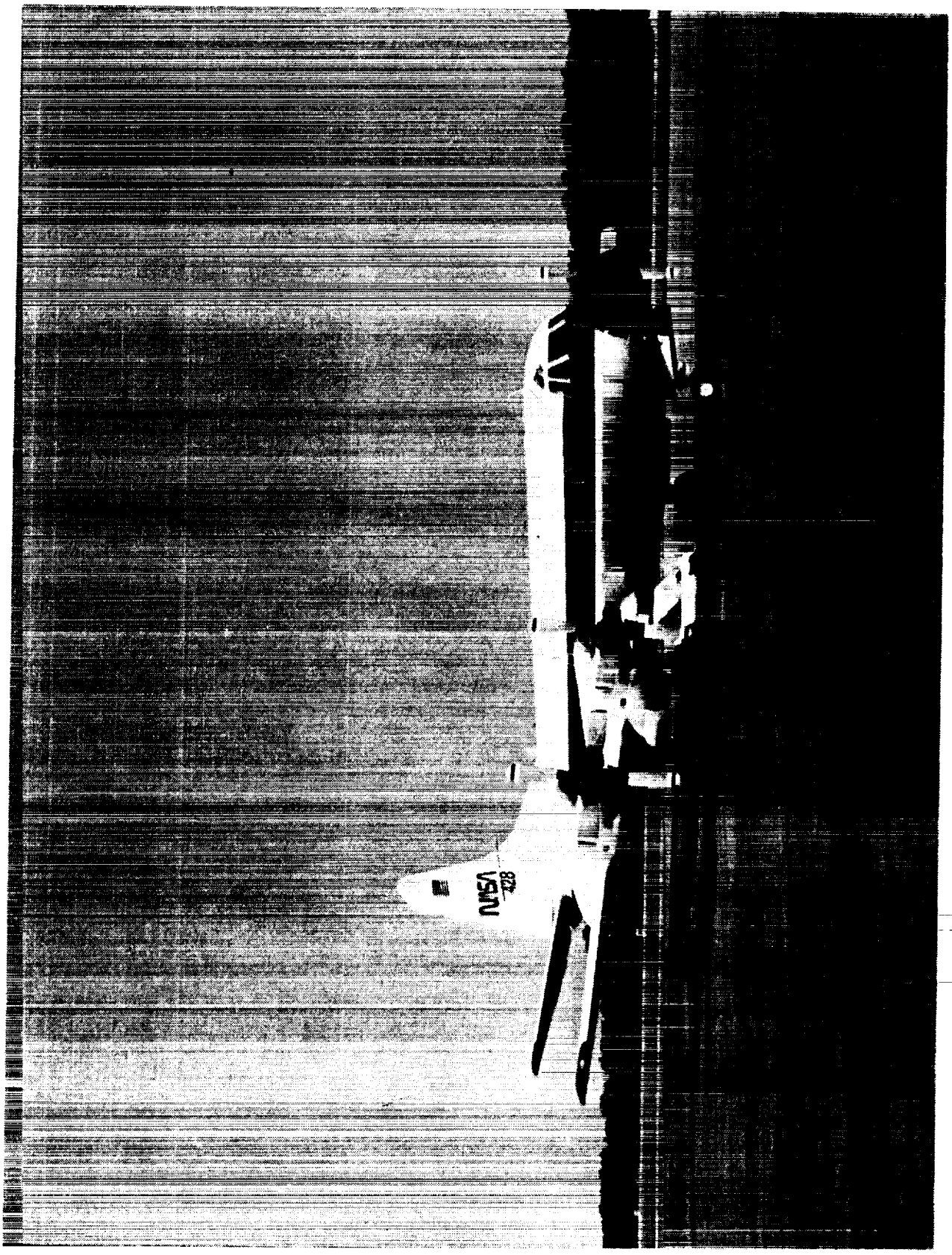


Figure 2. Lockheed P-3 vortex generating airplane.

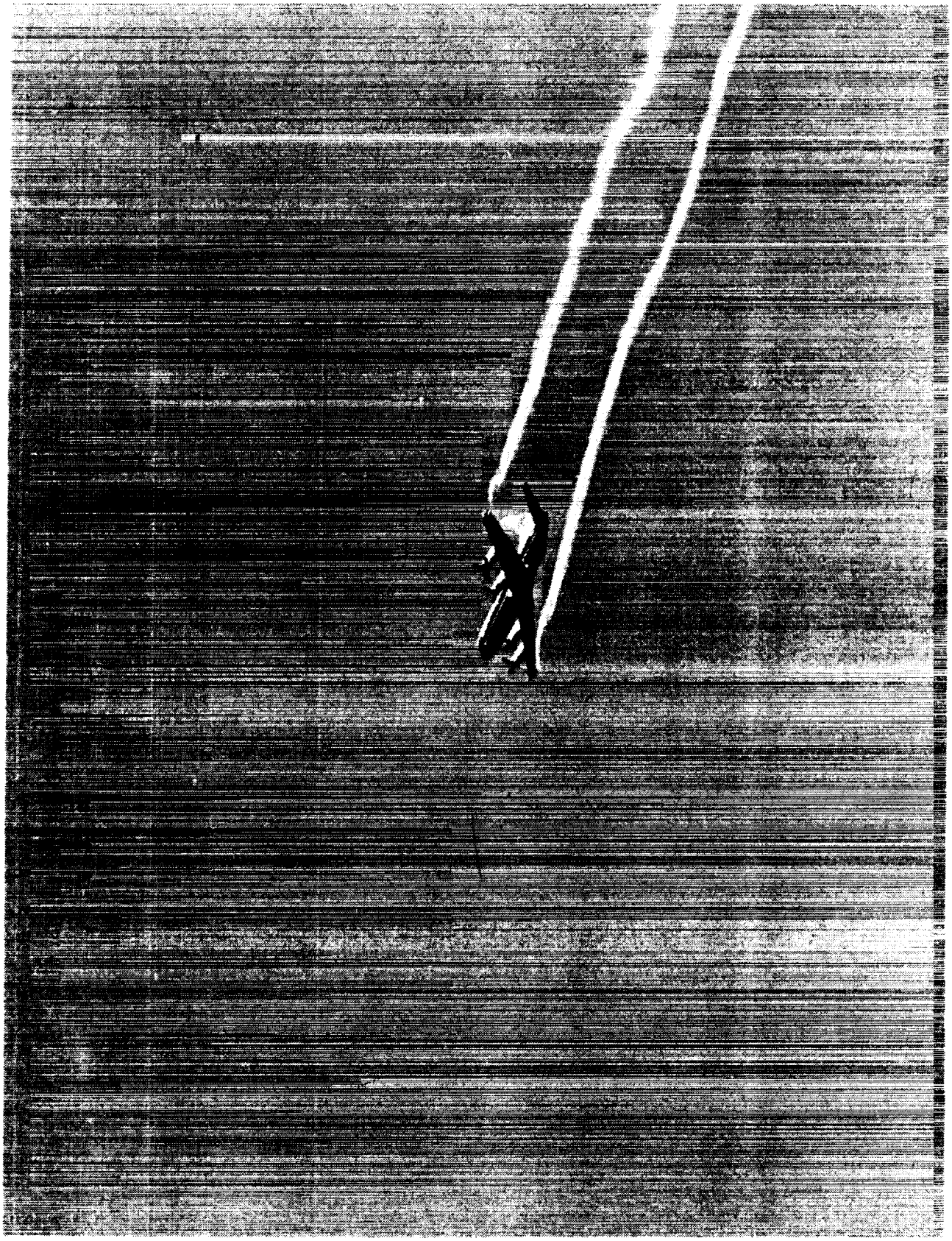

Figure 3. Visible vortex trails from smoke generators on the P-3 aircraft.

ORIGINAL PAGE
BLACK AND WHITE PHOTOGRAPH

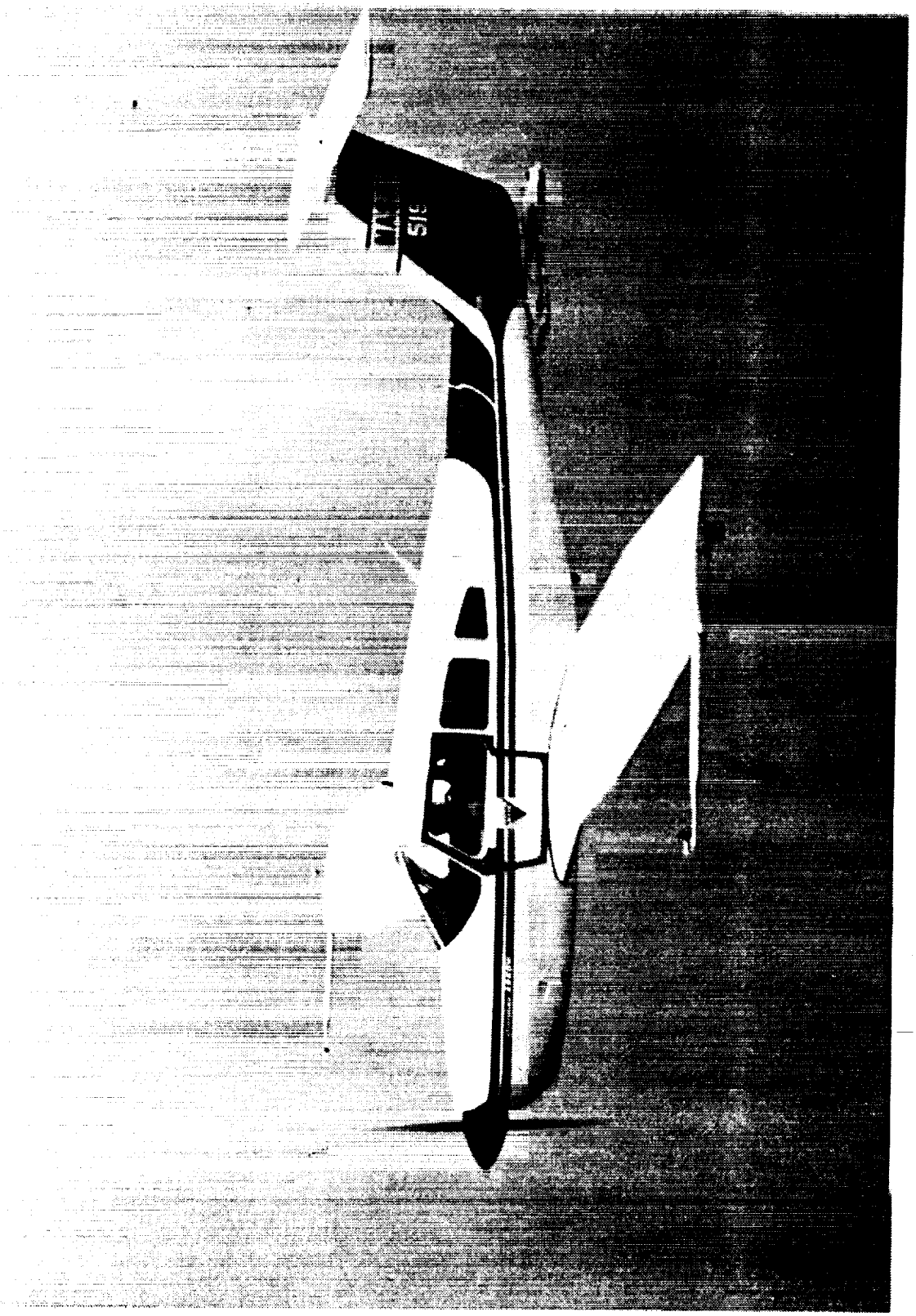

Figure 4. Piper PA-28 with probe mounted sensors to detect vortex flow.

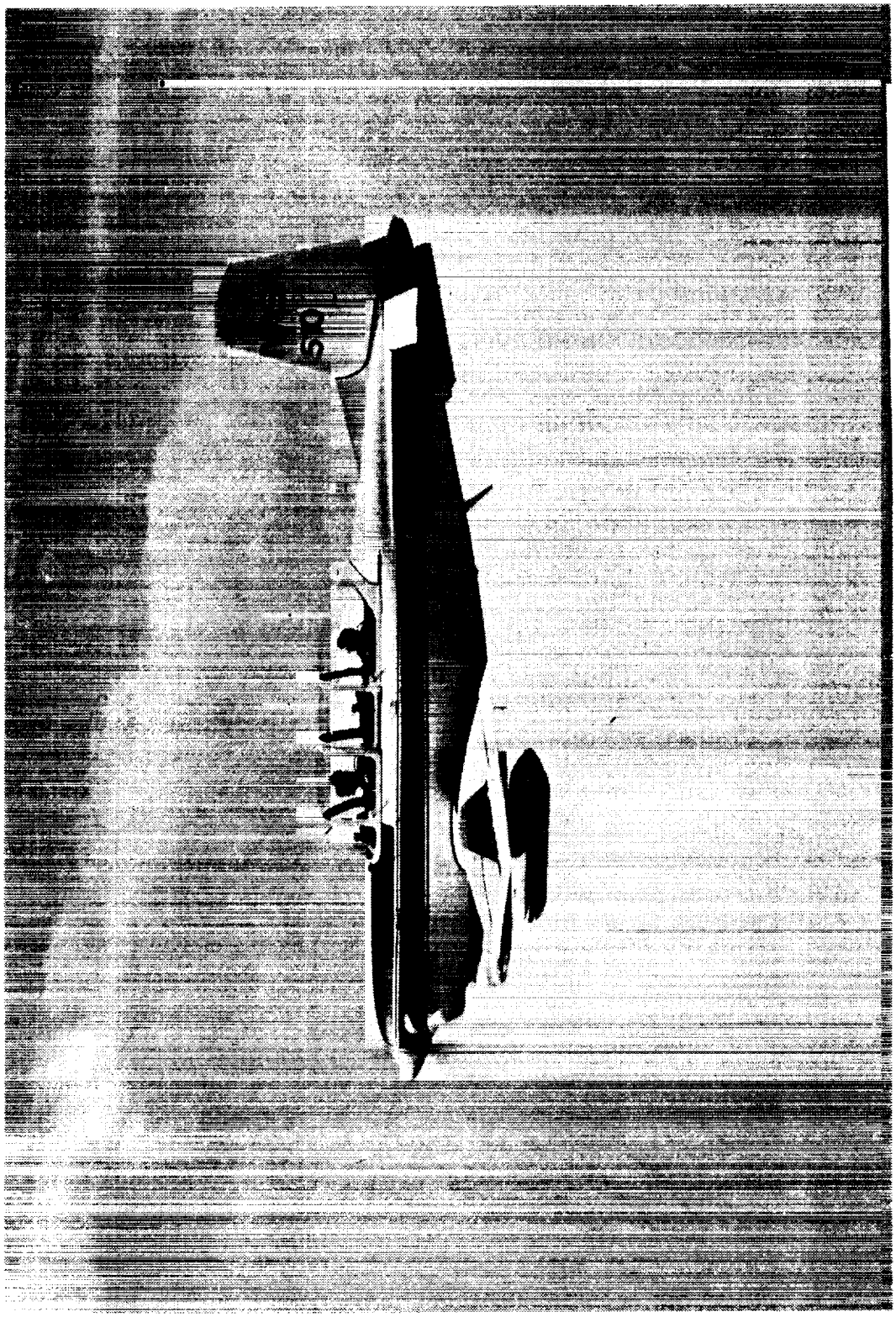

Figure 5. Beech T-34C photographic airplane.

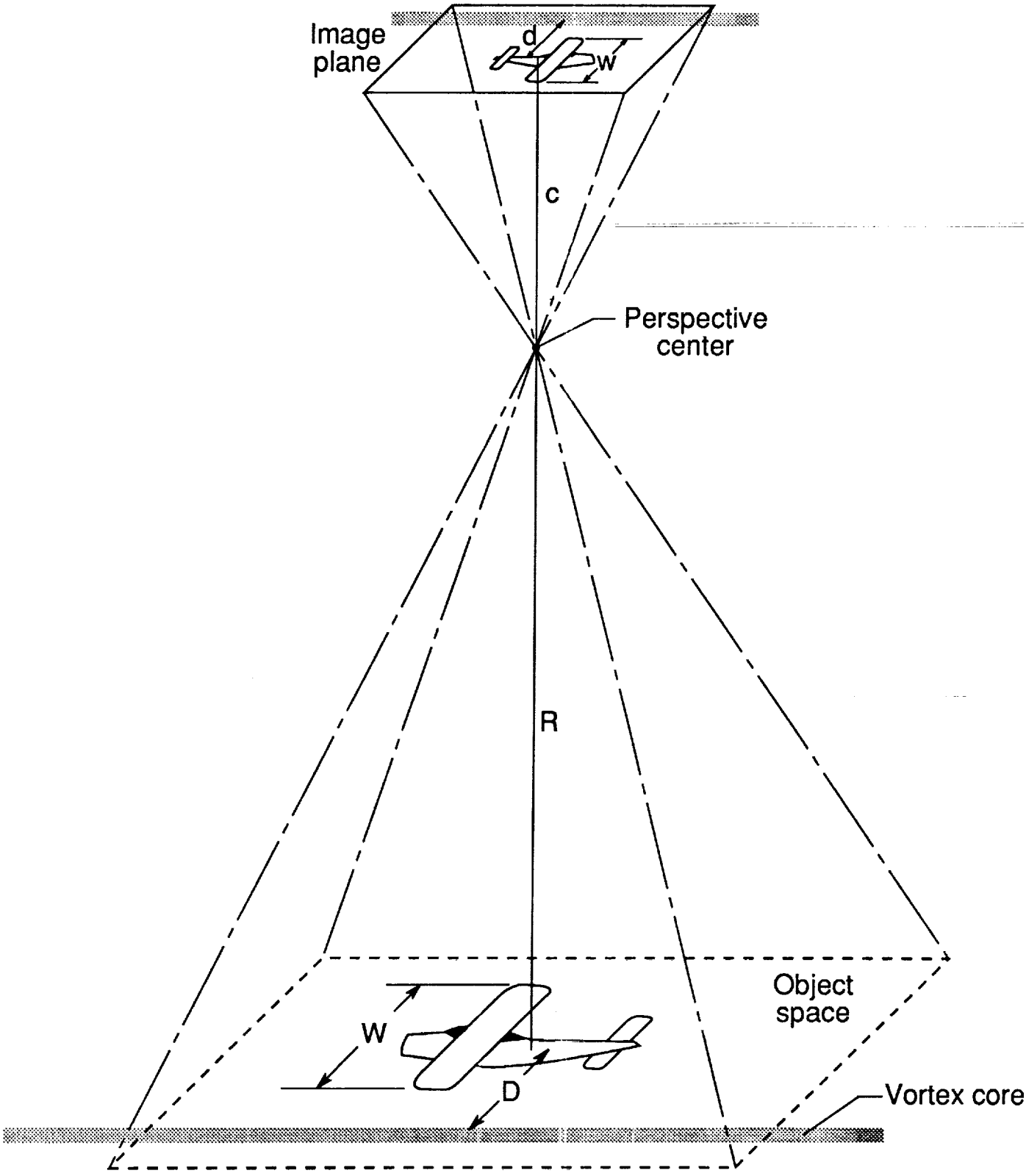


Figure 6. Geometry used to interpret photographs.

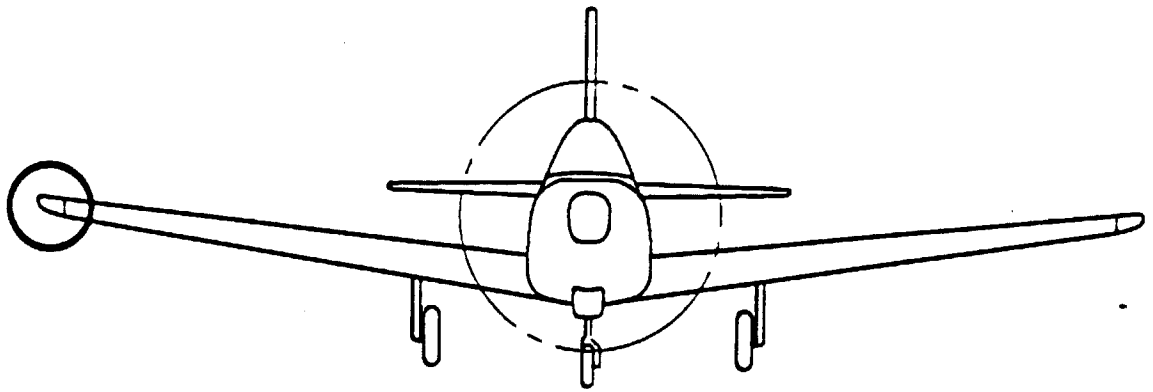

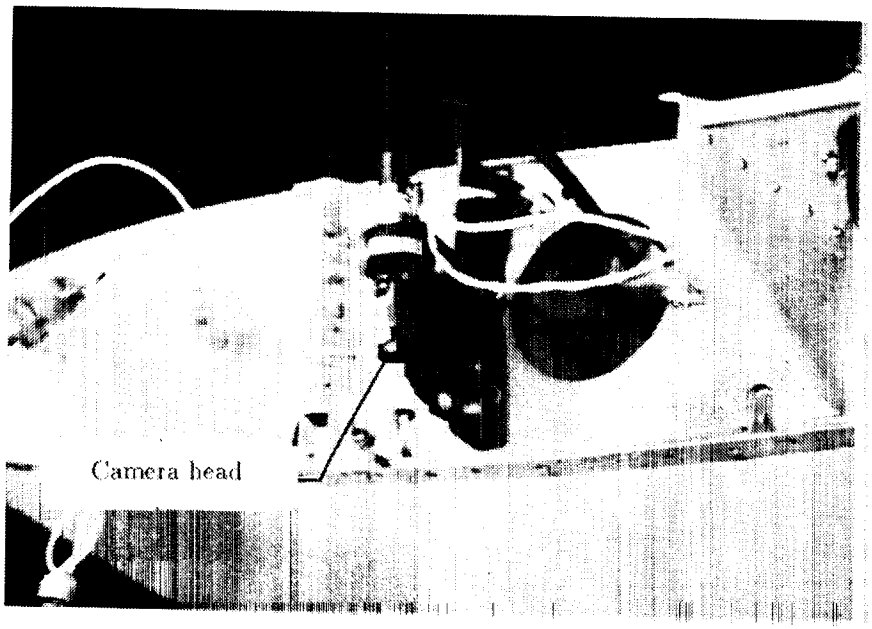


(a) Wing tip removed showing camera and mount

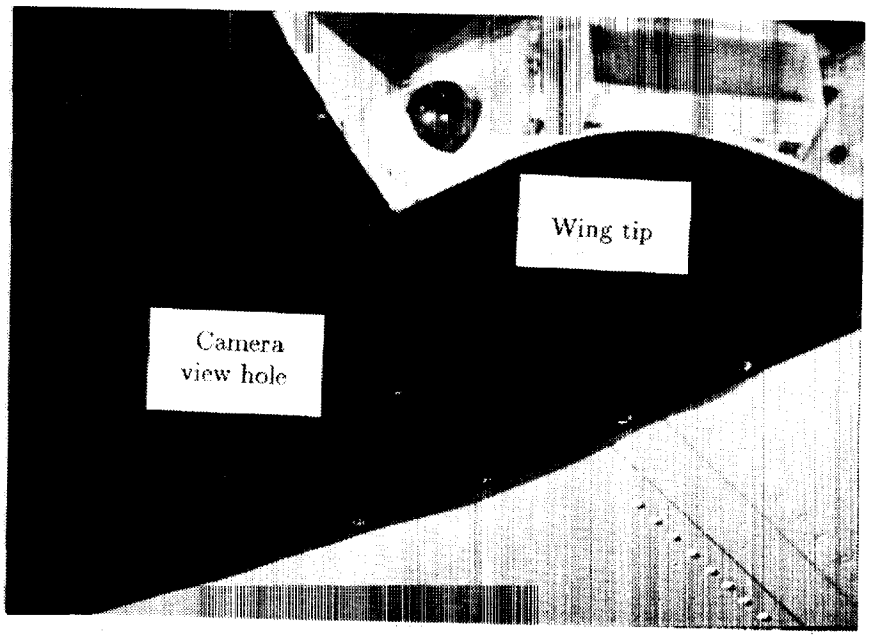


(b) Wing tip fairing installed showing opening for camera

Figure 7. Video camera location and mounting arrangement. The wing tip location for the right camera is circled in the sketch.

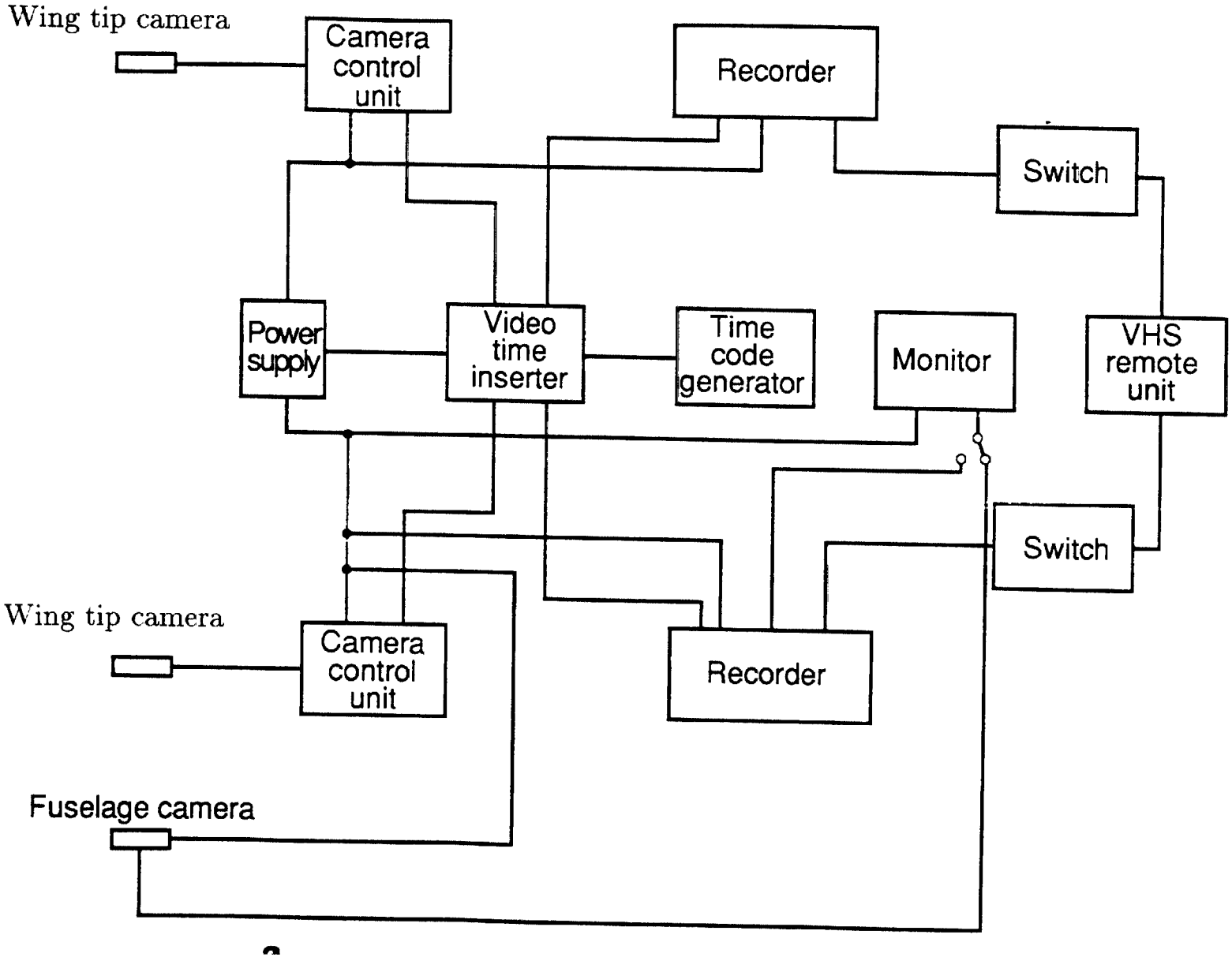


Figure 8. Schematic diagram of the camera system instrumentation on the T-34C airplane.

ORIGINAL PAGE
BLACK AND WHITE PHOTOGRAPH

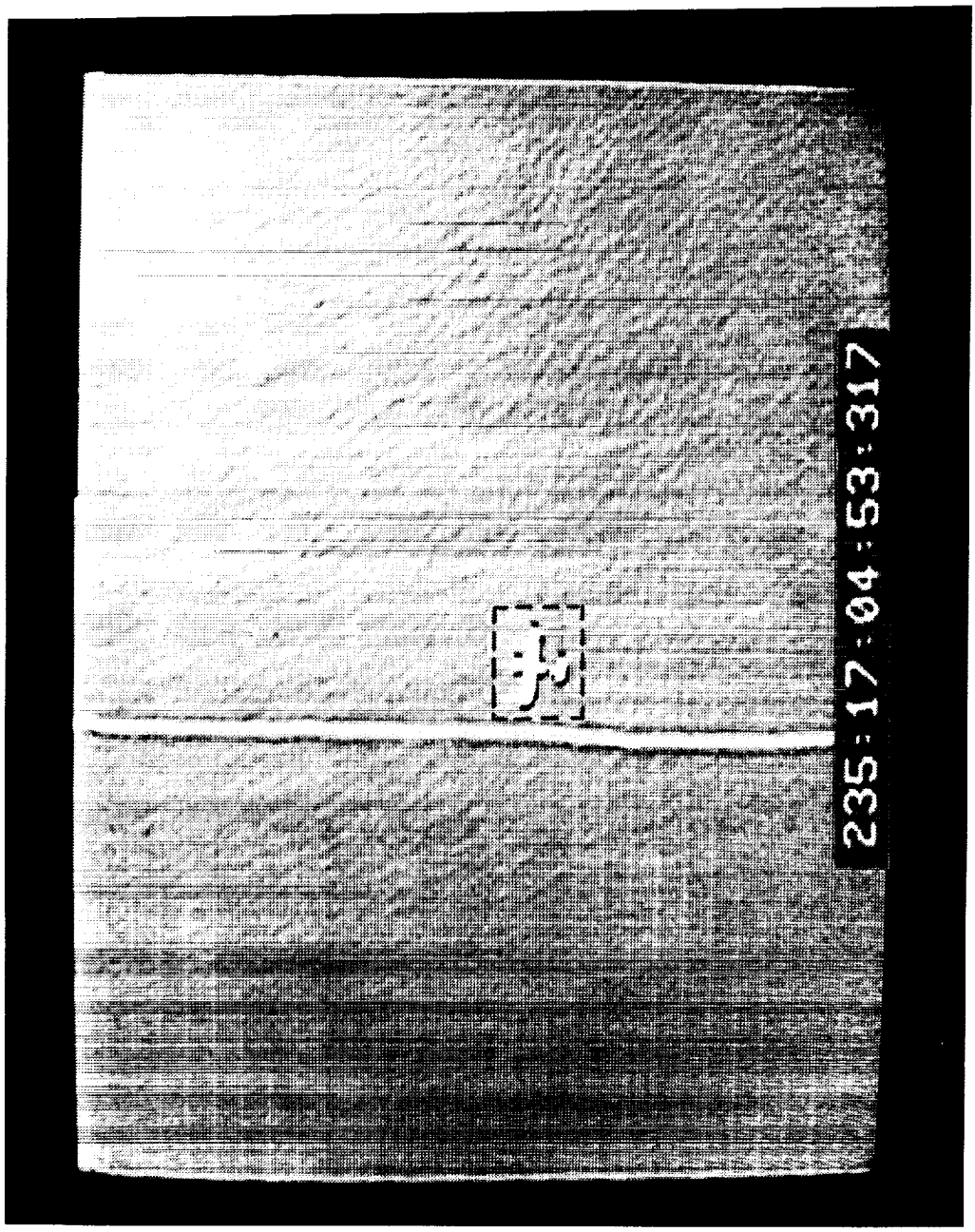


Figure 9. Typical video image from wing tip mounted camera showing the probe aircraft within a wingspan of the vortex core which is marked with smoke.

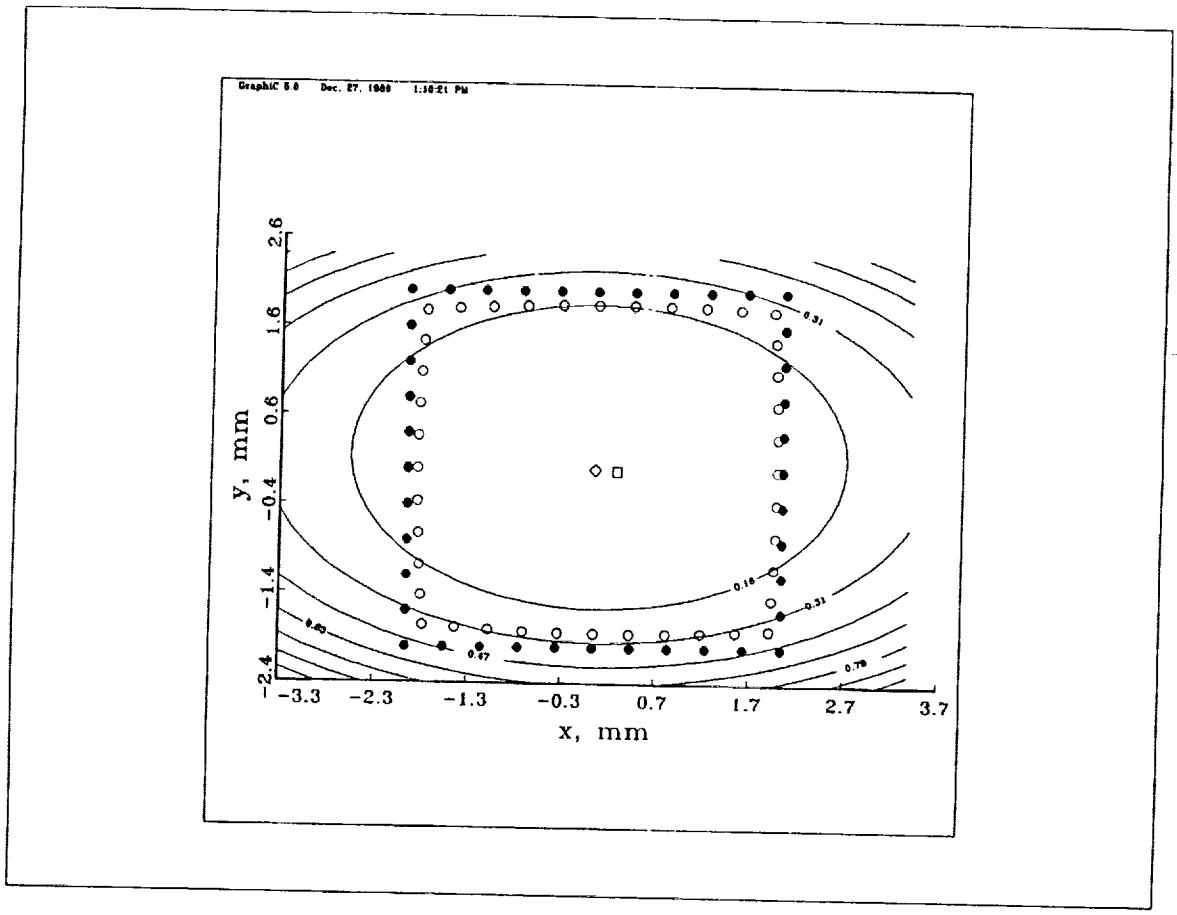


Figure 10. Contour plot of image distortion. The contour intervals correspond to 10 foot displacement error when scaled to the 500 foot working range of the experiment.

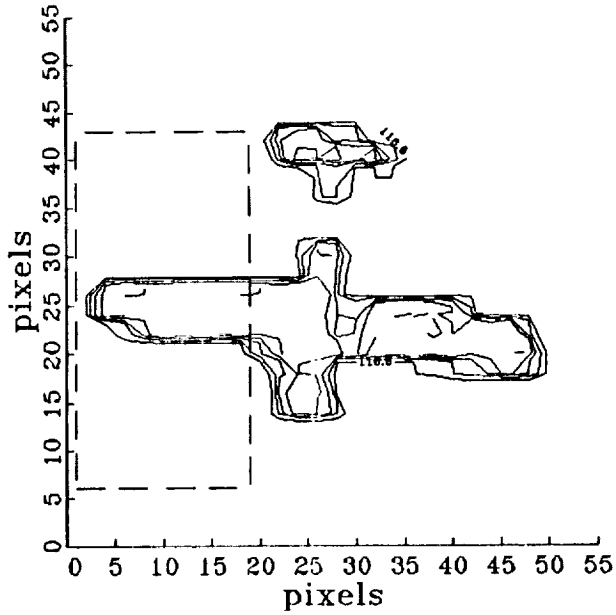


Figure 11. (a) Contour plot of pixel intensities surrounding the airplane image in figure 9. Minimum contour level chosen as 117.

| | | | | | | | | | | | | | | | | | | | |
|---|---|---|---|---|---|---|---|---|---|---|---|---|---|---|---|---|---|---|---|
| 90 | 82 | 84 | 95 | 94 | 80 | 82 | 87 | 88 | 79 | 81 | 90 | 85 | 79 | 82 | 89 | 86 | 78 | 80 | 88 |
| 91 | 82 | 84 | 96 | 94 | 80 | 82 | 87 | 88 | 79 | 81 | 89 | 86 | 78 | 82 | 89 | 87 | 78 | 79 | 88 |
| 83 | 91 | 96 | 88 | 86 | 92 | 93 | 82 | 81 | 88 | 91 | 81 | 82 | 89 | 90 | 80 | 81 | 88 | 91 | 82 |
| 84 | 91 | 96 | 88 | 85 | 92 | 94 | 82 | 82 | 88 | 92 | 81 | 82 | 89 | 90 | 80 | 80 | 89 | 91 | 82 |
| 93 | 90 | 84 | 86 | 91 | 85 | 79 | 82 | 88 | 81 | 75 | 79 | 87 | 83 | 81 | 85 | 93 | 88 | 83 | 85 |
| 93 | 90 | 84 | 87 | 91 | 85 | 79 | 82 | 88 | 81 | 75 | 79 | 87 | 84 | 81 | 85 | 93 | 89 | 83 | 85 |
| 83 | 88 | 94 | 91 | 82 | 82 | 89 | 88 | 80 | 82 | 91 | 92 | 89 | 88 | 95 | 93 | 85 | 84 | 89 | 90 |
| 83 | 87 | 94 | 91 | 82 | 82 | 89 | 89 | 80 | 82 | 91 | 92 | 89 | 88 | 95 | 92 | 86 | 84 | 89 | 90 |
| 94 | 94 | 84 | 82 | 90 | 89 | 81 | 81 | 88 | 92 | 88 | 87 | 92 | 90 | 82 | 81 | 85 | 77 | 67 | 77 |
| 94 | 94 | 84 | 82 | 91 | 89 | 81 | 81 | 89 | 93 | 87 | 87 | 93 | 90 | 81 | 82 | 85 | 77 | 67 | 77 |
| 87 | 83 | 87 | 92 | 86 | 82 | 91 | 95 | 84 | 83 | 92 | 90 | 79 | 81 | 92 | 93 | 76 | 71 | 84 | 83 |
| 88 | 82 | 87 | 93 | 87 | 82 | 91 | 95 | 84 | 83 | 92 | 90 | 79 | 80 | 92 | 93 | 75 | 71 | 84 | 82 |
| 90 | 99 | 94 | 89 | 90 | 97 | 93 | 86 | 91 | 99 | 94 | 86 | 92 | 101 | 97 | 85 | 87 | 95 | 88 | 69 |
| 90 | 99 | 94 | 90 | 90 | 97 | 93 | 86 | 91 | 99 | 94 | 86 | 92 | 102 | 97 | 85 | 87 | 96 | 88 | 69 |
| 93 | 87 | 88 | 97 | 101 | 89 | 84 | 91 | 94 | 83 | 84 | 95 | 97 | 85 | 86 | 95 | 97 | 92 | 105 | 132 |
| 93 | 87 | 88 | 97 | 100 | 89 | 85 | 90 | 94 | 83 | 84 | 94 | 97 | 85 | 86 | 95 | 97 | 92 | 105 | 132 |
| 79 | 91 | 109 | 108 | 105 | 115 | 129 | 142 | 168 | 200 | 223 | 217 | 207 | 212 | 220 | 213 | 206 | 213 | 218 | 212 |
| 78 | 91 | 109 | 107 | 105 | 115 | 129 | 141 | 168 | 199 | 223 | 217 | 207 | 213 | 220 | 213 | 206 | 213 | 218 | 212 |
| 80 | 93 | 116 | 162 | 197 | 215 | 209 | 204 | 219 | 219 | 207 | 202 | 213 | 216 | 213 | 210 | 216 | 217 | 208 | 208 |
| 80 | 94 | 116 | 161 | 198 | 216 | 209 | 204 | 219 | 219 | 206 | 202 | 213 | 215 | 213 | 210 | 216 | 217 | 208 | 208 |
| 57 | 57 | 112 | 167 | 192 | 203 | 209 | 210 | 201 | 195 | 197 | 205 | 206 | 206 | 211 | 214 | 212 | 207 | 208 | 210 |
| 57 | 56 | 110 | 167 | 192 | 202 | 209 | 210 | 201 | 194 | 196 | 205 | 206 | 206 | 211 | 214 | 212 | 207 | 208 | 210 |
| 73 | 76 | 84 | 97 | 92 | 88 | 75 | 61 | 55 | 54 | 49 | 46 | 49 | 46 | 44 | 42 | 38 | 35 | 29 | 19 |
| 73 | 76 | 84 | 97 | 92 | 88 | 75 | 62 | 55 | 54 | 49 | 46 | 48 | 46 | 44 | 42 | 38 | 35 | 29 | 18 |
| 86 | 83 | 88 | 93 | 90 | 81 | 74 | 72 | 67 | 59 | 62 | 64 | 62 | 61 | 69 | 77 | 78 | 75 | 81 | 85 |
| 86 | 83 | 88 | 92 | 89 | 81 | 74 | 72 | 67 | 59 | 62 | 64 | 63 | 61 | 69 | 78 | 79 | 76 | 82 | 85 |
| 93 | 95 | 91 | 87 | 88 | 88 | 85 | 82 | 83 | 86 | 85 | 83 | 88 | 90 | 94 | 89 | 87 | 91 | 92 | 87 |
| 92 | 96 | 91 | 86 | 88 | 88 | 86 | 82 | 83 | 86 | 85 | 83 | 87 | 90 | 94 | 89 | 87 | 90 | 93 | 87 |
| 97 | 92 | 82 | 85 | 90 | 87 | 87 | 92 | 92 | 92 | 88 | 96 | 98 | 95 | 91 | 90 | 93 | 94 | 94 | 90 |
| 97 | 92 | 82 | 86 | 90 | 88 | 87 | 92 | 92 | 92 | 88 | 97 | 98 | 96 | 91 | 90 | 93 | 94 | 95 | 91 |
| 81 | 82 | 90 | 88 | 82 | 87 | 90 | 86 | 80 | 86 | 90 | 85 | 81 | 83 | 89 | 88 | 87 | 85 | 90 | 88 |
| 81 | 82 | 89 | 88 | 81 | 86 | 90 | 86 | 80 | 86 | 91 | 85 | 81 | 83 | 89 | 88 | 86 | 85 | 90 | 88 |
| 82 | 88 | 80 | 77 | 84 | 87 | 80 | 80 | 87 | 90 | 83 | 82 | 88 | 90 | 84 | 83 | 87 | 89 | 86 | 85 |
| 82 | 88 | 80 | 78 | 84 | 87 | 80 | 80 | 85 | 90 | 84 | 82 | 88 | 90 | 84 | 83 | 86 | 88 | 85 | 85 |
| 90 | 81 | 81 | 92 | 90 | 80 | 82 | 91 | 89 | 78 | 81 | 90 | 88 | 80 | 82 | 89 | 86 | 73 | 76 | 90 |
| 90 | 81 | 82 | 92 | 90 | 80 | 82 | 91 | 88 | 78 | 82 | 90 | 89 | 81 | 82 | 89 | 86 | 73 | 76 | 90 |
| 81 | 84 | 87 | 81 | 79 | 87 | 93 | 85 | 80 | 87 | 93 | 83 | 81 | 89 | 95 | 79 | 68 | 77 | 87 | 77 |
| 81 | 84 | 87 | 81 | 79 | 86 | 92 | 85 | 80 | 86 | 92 | 83 | 80 | 89 | 94 | 79 | 67 | 76 | 87 | 77 |

Figure 11 (b) Listing of pixel intensities corresponding to the dashed area in part figure 11a.

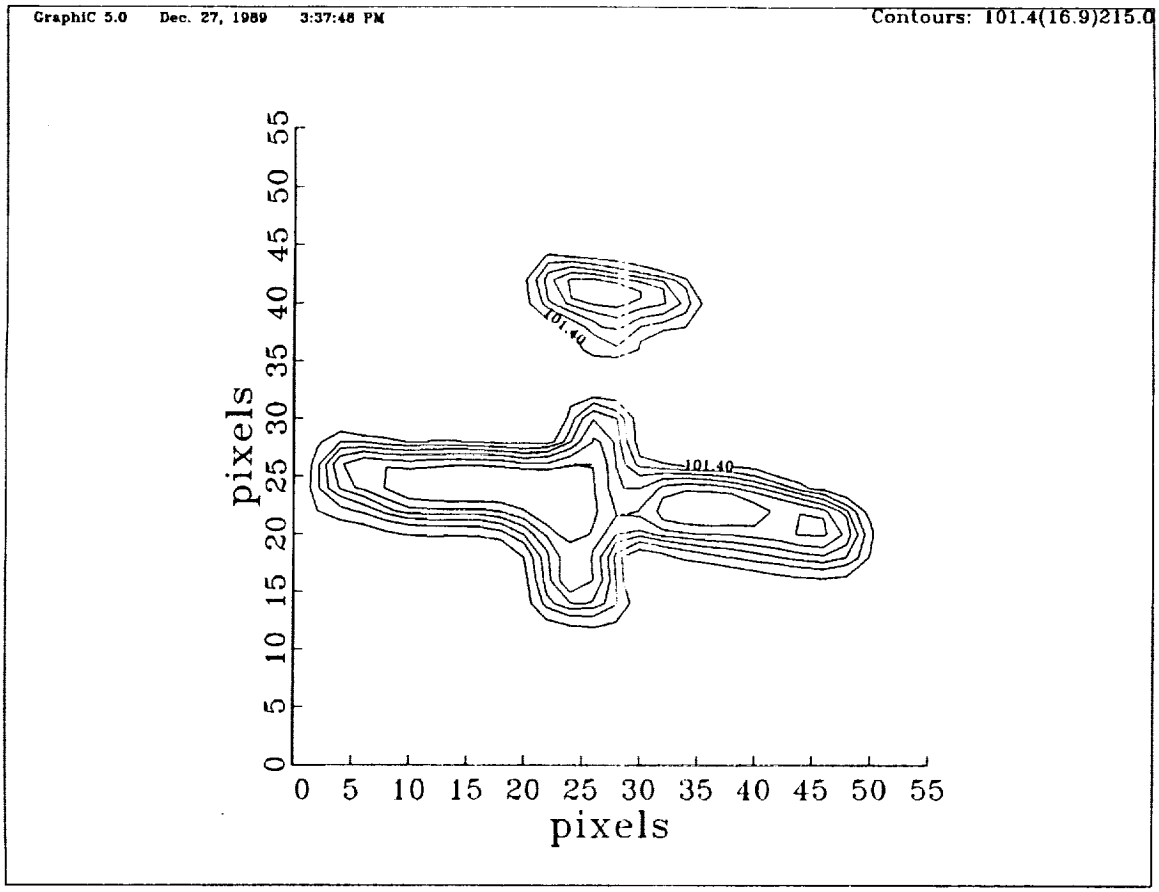


Figure 12. Contour plot of pixel intensities following nearest neighbor averaging of raw data.

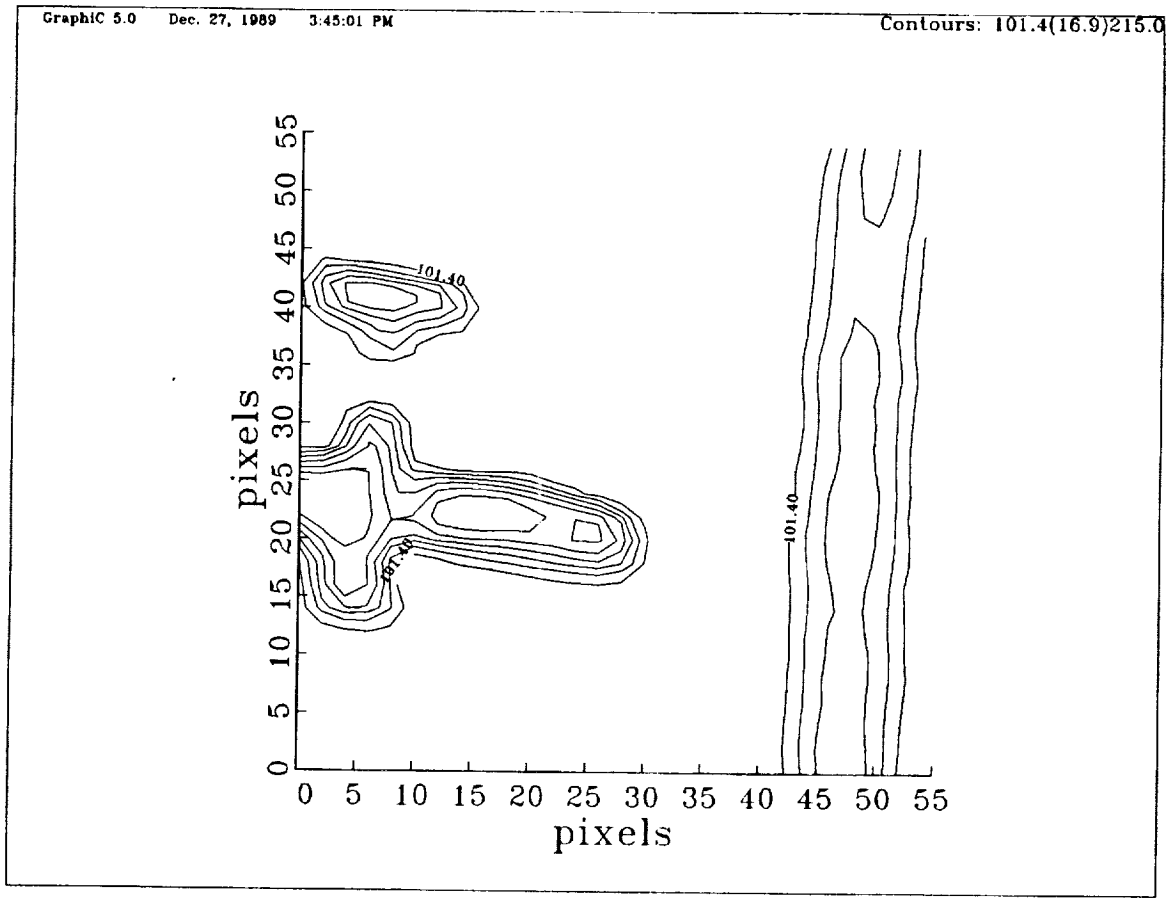


Figure 13. Contour plot of probe aircraft irradiance and vortex following nearest neighbor smoothing.

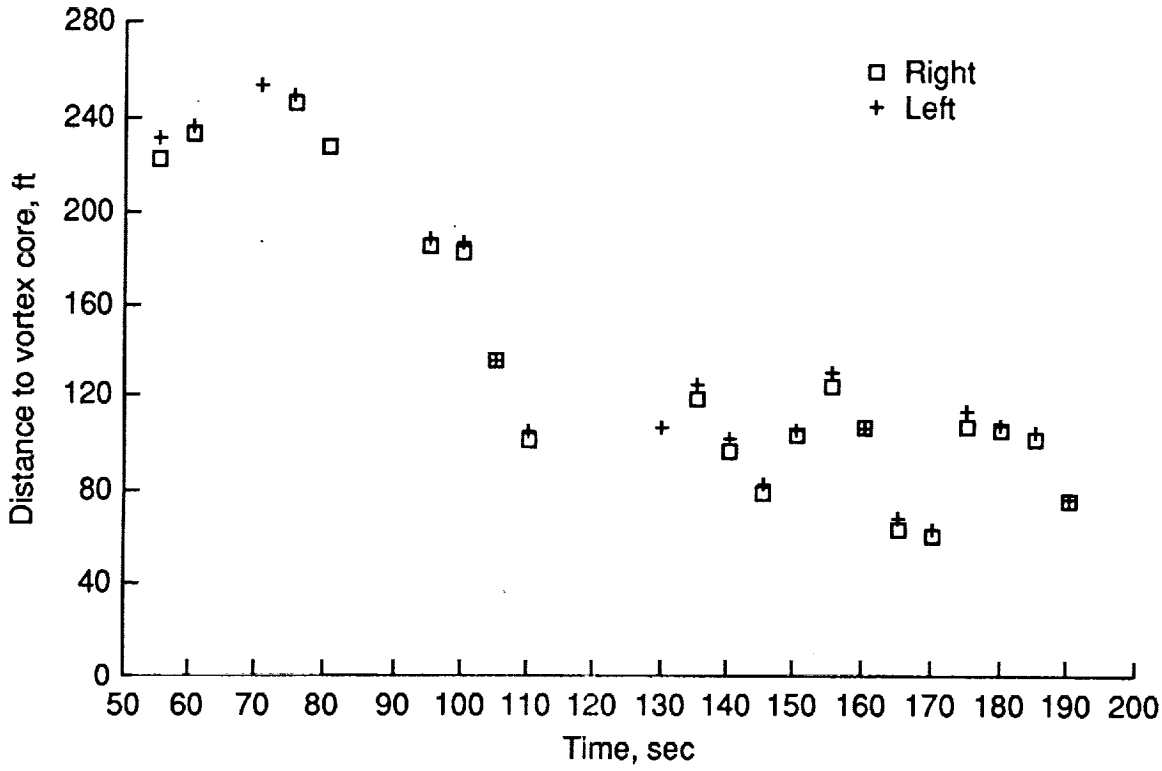


Figure 14. Plot to illustrate discrepancies of core distance measurements made by two different observers using data from separate wing tip cameras.

NASA National Aeronautics and Space Administration

# Report Documentation Page

| 1. Report No. | 2. Government Accession No. | 3. Recipient's Catalog No. |
|---|---|---|
| NASA TM-102691 | | |

**4. Title and Subtitle**
Video Photographic Considerations for Measuring the Proximity of a Probe Aircraft with a Smoke Seeded Trailing Vortex

**5. Report Date**
June 1990

**6. Performing Organization Code**

**7. Author(s)**
Brooks A. Childers and Walter L. Snow

**8. Performing Organization Report No.**

**10. Work Unit No.**
535-03-01-03

**9. Performing Organization Name and Address**
NASA Langley Research Center
Hampton, VA 23665-5225

**11. Contract or Grant No.**

**13. Type of Report and Period Covered**
Technical Memorandum

**12. Sponsoring Agency Name and Address**
National Aeronautics and Space Administration
Washington, DC 20546-0001

**14. Sponsoring Agency Code**

**15. Supplementary Notes**
Affiliated reports: NASA TM 102672 and FAA-PM-RD-90

**16. Abstract**

Considerations for acquiring and analyzing 30 Hz video frames from CCD cameras mounted in the wing tips of a Beech T-34 aircraft are described. Particular attention is given to the characterization and correction of optical distortions inherent in the data.

| 17. Key Words (Suggested by Author(s)) | 18. Distribution Statement |
|---|---|
| Video Image Analysis, CCD, Flight Testing, Vortex Detection | Unclassified - Unlimited<br>Subject Category 03 |

| 19. Security Classif. (of this report) | 20. Security Classif. (of this page) | 21. No. of pages | 22. Price |
|---|---|---|---|
| Unclassified | Unclassified | 23 | A03 |